Liu, W., Zhao, X., and Chen, Q. 2018. “A novel method for measuring air infiltration rate in buildings,” *Energy and Buildings*, 168: 309-319.

A Novel Method for Measuring Air Infiltration Rate in Buildings

Wei Liu[a,b], Xingwang Zhao[c], and Qingyan Chen[b,c*]

[a]School of Civil Engineering, ZJU-UIUC Institute, Zhejiang University, Haining 314400, China; [b]Center for High Performance Buildings, School of Mechanical Engineering, Purdue University, West Lafayette, IN 47907, USA; [c]Tianjin Key Laboratory of Indoor Air Environmental Quality Control, School of Environmental Science and Engineering, Tianjin University, Tianjin 300072, China

**Corresponding author:*
Email: yanchen@purdue.edu
Address: School of Mechanical Engineering, Purdue University, 585 Purdue Mall, West Lafayette, IN 47907-2088
Phone: (765) 496-7562, FAX: (765) 494-0539

Abstract

Measuring the air infiltration rate in buildings is essential for reducing energy use and improving indoor air quality. This rate has traditionally been determined by means of the blower door method, which is disruptive to building occupants, cannot identify the location of infiltration, cannot provide the infiltration rate for a section of the envelope, and requires considerable effort for setup and tear-down. Therefore, this study has developed a novel technique to measure air infiltration in buildings using an infrared camera. A thermographic image of a building envelope produced by an infrared camera and the measured indoor/outdoor air parameters (velocity, temperature, and pressure) were used to identify the effective crack size and air infiltration rate by means of theoretical heat transfer and fluid mechanics analyses. The proposed method was validated by experimental measurements in an environmental chamber and an office. The experiment in the environmental chamber constructed a small-scale room with known crack size. The experimental setup was comparable to actual conditions. The proposed method was able to predict the crack size within a relative error of 20%. For the experiment in the office, this study used the tracer-gas decay method to measure the air infiltration rate, and the relative error of the calculated air infiltration rate was only 3%.

Keywords: Air infiltration; Infrared camera; Thermography

1. Introduction

In 2015, approximately 40% of total U.S. primary energy or about 39 quadrillion BTU of energy was consumed in residential and commercial buildings [1]. Of the total primary energy used in buildings, 47% of it was for space heating and cooling [2]. The energy loss due to air infiltration through building cracks accounted for a significant portion of the energy consumed in buildings [3]. This portion may be as large as one-third of the energy used for heating and cooling in residential buildings [4] and 40% of the total heat energy demand in industrial buildings [5,6]. Similar results have been obtained in other studies [7-11]. Furthermore, air infiltration has a significant impact on indoor air quality, as it results in the transport of outdoor particles [12-14], gaseous contaminants [15], moisture [16,17], etc., into the indoor environment. Therefore, to reduce energy use and improve air quality inside buildings, it is essential to measure the air infiltration.

The traditional method of measuring air infiltration has been the use of a blower door [9,18-20]. A blower door is a powerful fan that is mounted on the frame of an exterior door. The fan pulls air out of or pushes air into a building, lowering or increasing the air pressure inside, which leads to airflow through buildings cracks and openings. By measuring the airflow rate through the blower under a given pressure difference between the indoor and outdoor spaces, one can determine the air infiltration rate through the building envelope [21]. Although the blower door method has been widely used, it

- is disruptive to building occupants,
- cannot provide the locations of infiltration,
- cannot be used to measure infiltration through a section of the envelope, and
- requires considerable effort for setup and tear-down.

Recently, new methods were developed to remedy the above-mentioned problems. Infrared thermography was integrated with the blower door method to identify the locations of building cracks [22]. Dufour et al. [23] further used infrared thermography to determine the size of artificial cracks. Since artificial cracks differ significantly from real cracks in buildings, knowing the size of an artificial crack is insufficient for determining the air infiltration rate. Qi [24] developed an inverse modeling method for estimating the air infiltration rate by comparing the monitored boiler gas consumption with the value calculated by use of the EnergyPlus model. However, the predicted air infiltration rate differed greatly from that measured by the blower door test. To fully remedy the above-mentioned problems, further investigation is required. Therefore, this study has developed a novel diagnostic technique for air infiltration in buildings using an infrared camera. To validate the method, we obtained experimental data on the infiltration rate in an environmental chamber and an office.

2. Method development

Air infiltration through cracks in a section of a building envelope is a function of the surface temperature and the pressure and temperature differences between indoor and outdoor spaces. The function can be determined by heat transfer and fluid mechanics analyses. This study first assumed a simplified building crack as shown in Figure 1. The dimensions of the crack are $D \times L_c$ (length × height) in this two-dimensional figure.

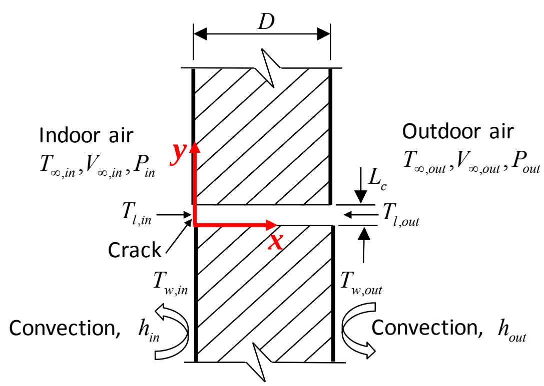

Figure 1. Simplified model for a crack in a section of a building envelope.

The flow through the crack is assumed to be:

- Steady-state: $\partial()/\partial t = 0$
- Two-dimensional planar flow: $\mathrm{w} = 0,\ \partial()/\partial z = 0$, where z is the third direction
- Fully developed flow, since $D >> L_c$: $\partial u/\partial x = 0, \partial v/\partial x = 0$
- Constant properties: ρ, μ

where u, v, and w are the air velocity in the x, y, and z directions, respectively, t is time, ρ is the air density, and μ is the dynamic viscosity. Then the Navier-Stokes equations that govern the airflow through the crack can be simplified as

$$\frac{\partial v}{\partial y} = 0 \tag{1}$$

$$\rho \mathrm{v} \frac{\partial u}{\partial y} = \mu \frac{\partial^2 u}{\partial y^2} - \frac{\partial P}{\partial x} \tag{2}$$

$$\rho \mathrm{v} \frac{\partial v}{\partial y} = \mu \frac{\partial^2 v}{\partial y^2} - \frac{\partial P}{\partial y} \tag{3}$$

The corresponding boundary conditions are:

$$\mathrm{u}(\mathrm{y} = 0, \mathrm{y} = L_c) = 0 \tag{4}$$

$$\mathrm{v}(\mathrm{y} = 0, \mathrm{y} = L_c) = 0 \tag{5}$$

$$\mathrm{P}(\mathrm{x} = 0) = P_{in} \tag{6}$$

$$\mathrm{P}(\mathrm{x} = \mathrm{D}) = P_{out} \tag{7}$$

With all the above assumptions and boundary conditions, we have

$$u(y) = \frac{\Delta P}{2\mu D} y^2 - \frac{\Delta P L_c}{2\mu D} y \quad (8)$$

$$u_m = \int_{y=0}^{y=L_c} u(y) dy / L_c = -\frac{\Delta P L_c^2}{12\mu D} \quad (9)$$

At the same time, the flow through the crack would affect the temperature distribution on the wall. This investigation assumed the heat dissipated by the leaked air to be equal to the summation of the heat convection between the wall and the indoor/outdoor air. We neglected the heat conduction in the vertical direction within the wall and the effect of solar radiation. Thus, we have

$$u_m L_c \rho C_p (T_{l,out} - T_{l,in}) = Q_{in} + Q_{out} \quad (10)$$

$$Q_{in} = h_{in} A (T_{\infty,in} - T_{w,in}) \quad (11)$$

$$Q_{out} = h_{out} A (T_{\infty,out} - T_{w,out}) \quad (12)$$

where $T_{l,in}$ and $T_{l,out}$ are the leaked air temperature at the left and right ends of the crack, respectively (refer to Figure. 1), h_{in} and h_{out} are heat convective coefficients, A is the wall area, $T_{\infty,in}$ and $T_{\infty,out}$ are the ambient indoor and outdoor air temperature, and $T_{w,in}$ and $T_{w,out}$ are the inside and outside mean wall temperature. From Eq. 10, we have

$$Q_f = \frac{Q_{in} + Q_{out}}{\rho C_p (T_{l,out} - T_{l,in})} \quad (13)$$

By combining Eq. 9 with Eq. 10 to eliminate u_m, we obtain the crack height L_c:

$$L_c = \left[\frac{12\mu D (Q_{in} + Q_{out})}{\Delta P \rho C_p (T_{l,in} - T_{l,out})} \right]^{1/3} \quad (14)$$

The above equation is for a crack with unit width. If the width of the crack is W, then the crack size is

$$L_c = \left[\frac{12\mu D (Q_{in} + Q_{out})}{\Delta P \rho C_p W (T_{l,in} - T_{l,out})} \right]^{1/3} \quad (15)$$

To apply Eqs. 13 and 14, one must measure the following parameters:

- Wall temperature distribution by infrared camera to obtain $T_{w,in}$ and $T_{w,out}$,
- Indoor and outdoor ambient air temperature $T_{\infty,in}$ and $T_{\infty,out}$,
- Indoor-outdoor pressure difference ΔP, and
- Indoor and outdoor air velocity $V_{\infty,in}$ and $V_{\infty,out}$ in order to calculate h_{in} and h_{out}

The specific measurement locations are hard to identify, but we recommend measuring multiple locations that are close to the target building envelop and using the average value. To determine the wall heat convection coefficient, the room height, H, is used as the characteristic length. Then the Reynolds number is

$$Re_{in} = \frac{\rho V_{\infty,in} H}{\mu} \quad (16)$$

$$Re_{out} = \frac{\rho V_{\infty,out} H}{\mu} \tag{17}$$

This study assumed the flow over the wall surface to be parallel flow over an isothermal flat plate, and the critical Reynolds number to be Re_c = 10^5~3×10^6. The following two empirical correlations (Eq. 18 for laminar flow and Eq. 19 for mixed boundary layer conditions) [25] can be applied to determine the average Nusselt number $\overline{Nu}$:

$$\overline{Nu} = \frac{\bar{h}H}{k} = 0.644 Re_H^{1/2} Pr^{1/3} \tag{18}$$

$$\overline{Nu} = \frac{\bar{h}H}{k} = (0.037 Re_H^{4/5} - B) Pr^{1/3} \tag{19}$$

$$B = 0.037 Re_c^{4/5} - 0.644 Re_c^{1/2} \tag{20}$$

where k is the heat conduction coefficient and Pr is the Prandtl number. Hence, the heat convection coefficient h_{in} and h_{out} can be determined. Please note that the wall can be vertical, horizontal, or angled.

3. Method validation

To validate the infiltration determination method above, this study conducted experimental measurements of the infiltration rate in an environmental chamber and an office. The environmental chamber created ideal, desirable indoor/outdoor environments, while the office was used to demonstrate the applicability of the proposed method to a realistic case.

3.1 Experiment in an environmental chamber

The environmental chamber was located in the Ray W. Herrick Laboratories at Purdue University. Figure 2 shows the overall layout of the facility, which consisted of two rooms. The larger room was a test chamber with dimensions of 4.8 *m* × 4.2 *m* × 2.4 *m* that was used to simulate the outdoor environment in this experiment. Two air supply diffusers on the floor of the chamber and one exhaust on the ceiling were used to maintain a stable thermo-fluid environment. Inside the test chamber, we constructed a box with dimensions of 0.5 *m* × 0.5 *m* × 0.5 *m* to simulate a small indoor environment. One of the walls of the box had an artificial crack with dimensions of 0.5 *m* × 18 *mm* × 1 *mm* ($x \times y \times z$). The box was connected to the climate chamber by a duct, through which air at different temperatures in the climate chamber was supplied to the box; the air then leaked back into the test chamber through the crack.

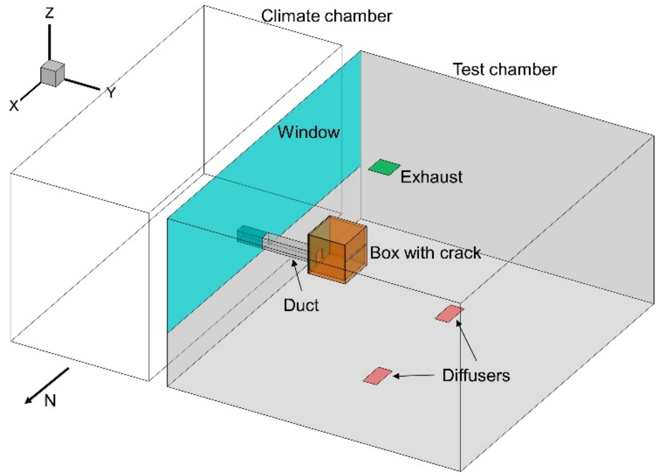

Figure 2. Schematic view of the experimental setup in an environmental chamber.

Figure 3(a) shows an external view of the small box and duct. The duct was insulated with foam core and aluminum foil. The duct contained a flow meter, a valve, an air compressor, and a heater. Figure 3(b) shows the other side of the box, which was made of plexiglass. The upper part of the plexiglass wall was removable, so that the temperature distribution on the inside wall of the box could be measured. This study installed eight thermocouples to monitor the inside wall temperature of the box and four thermocouples along the duct to monitor the supply air temperature. A manometer was used to measure the inside-outside pressure difference. We conducted repeated measurements for six scenarios with varying air infiltration rate and heater power (Table 1). For all the scenarios, the airflow rate for the test chamber was 7.7 ACH, and the air supply temperature for the test chamber was controlled at 15 ^{o}C.

(a) (b)

Figure 3. Details of the experimental setup: (a) the box and duct and (b) removable wall made of plexiglass.

Table 1. Summary of the experimental scenarios

Scenario	1	2	3	4	5	6
Heater power (*W*)	25			40		
Air infiltration rate (*L/min*)	25	50	75	25	50	75
ACH (h^{-1})	1.2	2.4	3.6	1.2	2.4	3.6

Using Scenario 1 as an example, Figure 4 shows the box wall temperature and the supply air temperature from the duct. We ran the system for at least five hours before conducting the measurements at 16:30. This study also measured the outside air velocity and temperature with the use of omni-directional hot-sphere anemometers, the inside-outside pressure difference with a manometer (range: +/- 0.2 inch of water and accuracy: +/- 1% of range), and the temperature distribution on the box wall with the crack with an infrared camera.

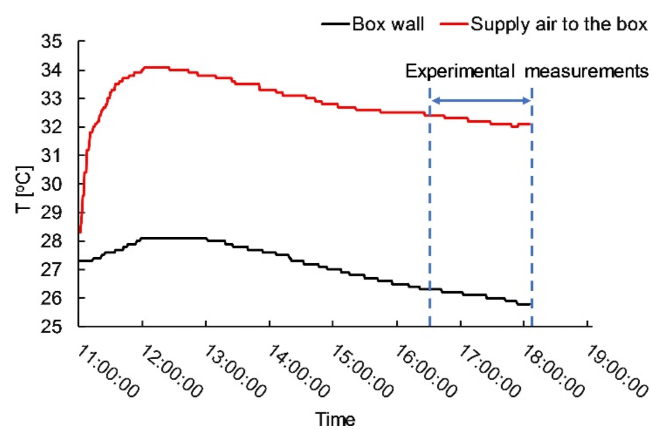

Figure 4. The box wall temperature and the supply air temperature from the duct.

We obtained the following data:

- *Wall temperature distribution:* Figure 5 shows the outside and inside temperature distributions on the surfaces of the wall with the crack. The outside and inside mean wall temperatures were $T_{w,out} = 24.2\ ^oC$ and $T_{w,in} = 25.7\ ^oC$, respectively.
- *Indoor and outdoor ambient air temperatures:* $T_{\infty,in} = 26.8\ ^oC$ and $T_{\infty,out} = 23.1\ ^oC$.
- *Indoor-outdoor pressure difference:* $\Delta P = 1.0\ Pa$. The inside air pressure was higher than the outside air pressure, and thus exfiltration occurred. Therefore, this study

assumed that $T_{l,in} = T_{\infty,in}$ and $T_{l,out}$ = 25.4 ^oC, which was determined from the thermographic image in Figure 5(a).

- *Indoor and outdoor air velocities:* The measured mean air velocity outside the box was $V_{\infty,out}$ = 0.1 *m/s*. For the indoor velocity, it was impossible to place a hot-sphere anemometer inside the box. We estimated the mean air velocity by dividing the air infiltration rate by the area of the box wall and obtained $V_{\infty,in}$ = 0.019 *m/s*. Using the box height as the characteristic length, H = 0.5 *m*, yielded Reynolds numbers of Re_{in} = 630 and Re_{out} = 3300. The flow was laminar, and Eq. 18 was applied to determine the average Nusselt number. The calculated convective heat coefficients were h_{in} = 0.74 $W/(m^2K)$ and h_{out} = 1.69 $W/(m^2K)$.

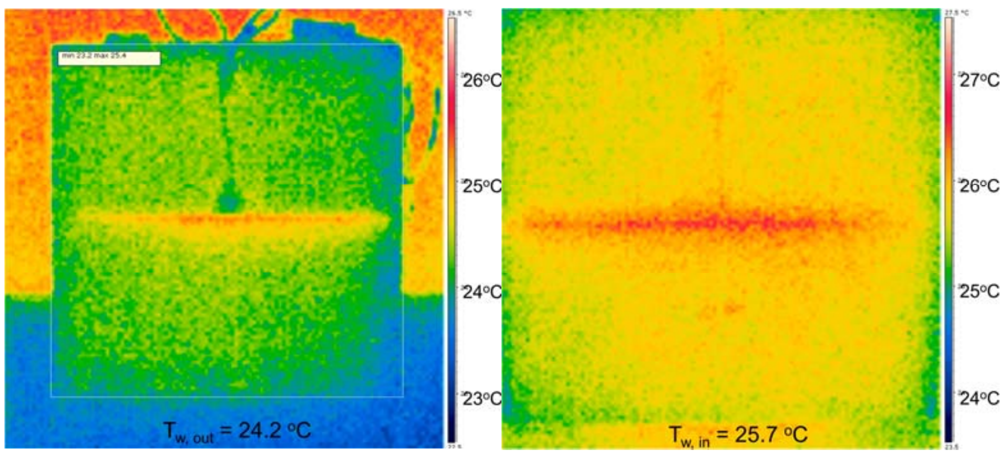

(a) (b)

Figure 5. Temperature distribution on the box wall surfaces with the crack: (a) outside and (b) inside.

Using the above-mentioned numbers and Eq. 14, we calculated the crack height as $L_{c,calculated}$ = 1.15 *mm* for Scenario 1, while the actual size was $L_{c,actual}$ = 1.0 *mm*. The relative error was 15%. Table 2 summarizes the crack height as calculated by Eq. 14 for the six scenarios. When the air exfiltration rates were 25 *L/min* and 50 *L/min*, our proposed method was able predict the crack height with a relative error of less than 20%. When the air exfiltration rate was 75 *L/min*, the method failed to accurately predict the crack height. Possible reasons for this failure will be presented in the discussion section of this paper.

Table 2. Crack height for the various scenarios as calculated by the proposed method.

Scenario	1	2	3	4	5	6
$L_{c,calculated}$ (*mm*)	1.15	0.92	0.63	1.05	0.93	0.62
Relative error*	15%	8%	37%	5%	7%	38%

*$L_{c,actual}$ = 1.0 mm

3.2 Experiment in an office

To investigate the performance of the proposed method under realistic conditions, we used the method to calculate the air infiltration rate in an office as shown in Figure 6. The office was 7.35 *m* long, 3.5 *m* wide, and 3.12 *m* high. It was located on the second floor of a three-story building with a south-facing exterior wall and window, on the campus of Tianjin University, Tianjin, China. This study assumed that air infiltration occurred through cracks in and around the window, since the door was interior door and kept closed during the experiment.

Figure 6. Inside view of the office and SF_6 sampling locations, with the SF_6 source released at the position from which this photo was taken.

The test was conducted at night to avoid the effect of solar radiation on the window. The air conditioner blew hot air during the test. The outdoor air temperature was around 20 ^oC in September 2017, and thus the indoor-outdoor air temperature difference was minimal. We used a HOBO data logger and thermocouples to measure the indoor and outdoor air temperatures, omni-directional hot-sphere anemometers to measure the indoor and outdoor air velocities, a manometer (range: +/- 25 Pa and accuracy: +/- 0.4% of range) to measure the indoor-outdoor pressure difference, and an infrared camera to measure the temperature distribution on the external wall. The measurements were conducted after the air-conditioner had run for three hours. We collected the following experimental data:

- *Wall temperature distribution:* Figure 7 shows the measured temperature distributions on the inside and outside of the external wall and window surfaces.

The inside and outside mean wall temperatures were $T_{w,in}$ = 29.9 ^oC and $T_{w,out}$ = 24.6 ^oC, respectively.

- *Indoor and outdoor ambient air temperatures:* Figure 8 shows the measured indoor and outdoor air temperatures. The measurements were conducted around midnight, when $T_{\infty,in}$ = 31.2 ^oC and $T_{\infty,out}$ = 22.9 ^oC, respectively.
- *Indoor-outdoor pressure difference:* The difference was ΔP = 0.3 Pa, where the outside air pressure was higher than the inside air pressure. Infiltration occurred, so that $T_{l,out}$ = $T_{\infty,out}$ and $T_{l,in}$ = 24.6 ^oC, where $T_{l,in}$ was determined from the thermographic image in Figure 7(b).
- *Indoor and outdoor air velocities:* The measured mean air velocities for the indoor and outdoor air were $V_{\infty,in}$ = 0.41 m/s and $V_{\infty,out}$ = 0.56 m/s, respectively. For the indoor air, this study used the height of the office as the characteristic length, H = 3.12 m, and the corresponding Reynolds number was Re_{in} = 8.5×10^4. At this Re, the flow was laminar. Therefore, we used Eq. 18 to determine the average Nusselt number. Furthermore, the calculated heat convection coefficient was h_{in} = 1.41 $W/(m^2K)$. For the outdoor air, this study again used the height of the office as the characteristic length. However, since the office was on the second floor, Eqs. 18 and 19 could not be applied directly. This study first calculated the mean Nusselt number for the first floor with H_1 = 3.12 m and $Re_{1,out}$ = 1.2×10^5. Using $Re_c = 10^5$ and Eq. 19, we obtained $Nu_{1,out}$ = 227 and $h_{1,out}$ = 1.87 $W/(m^2K)$. This study then considered the first and second floors together with H_2 = 6.24 m. In the same way, the corresponding mean heat convection coefficient was $h_{2,out}$ = 2.06 $W/(m^2K)$. Finally, the mean heat convection coefficient for the second floor was $h_{out} = (h_{2,out}H_2 - h_{1,out}H_1)/(H_2 - H_1)$ = 2.25 $W/(m^2K)$.

With the above data and Eq. 14, this study determined the air infiltration rate to be $Q_{f,calculated}$ = 24.95 m^3/h.

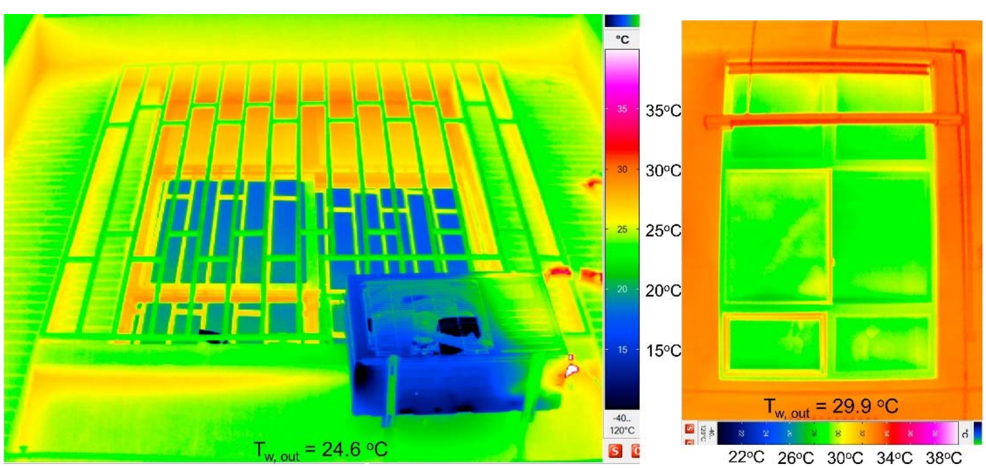

(a) (b)

Figure 7. Temperature distributions on the external wall: (a) outside surface and (b) inside surface.

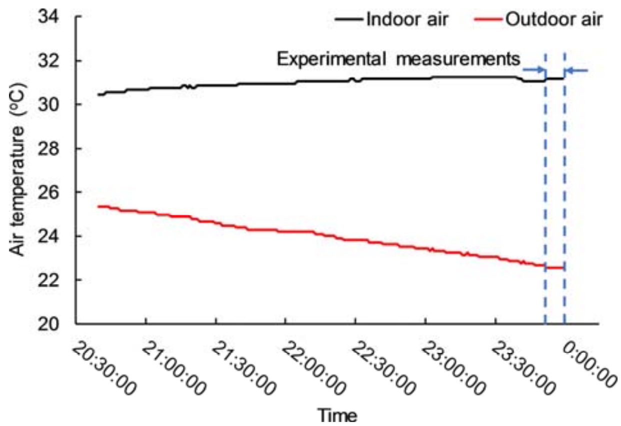

Figure 8. Measured indoor and outdoor air temperatures.

To validate the calculated air infiltration rate in the office, this study applied the tracer-gas decay method using a photoacoustic gas analyzer (model INNOVA 1412) to measure the air infiltration rate. The tracer gas, SF_6, was released for about one hour and decayed for two hours. We sampled the SF_6 concentration at three locations (indicated in Figure 6) to ensure that the tracer gas was well-mixed in the room. Figure 9(a) shows the measured SF_6 concentration versus time. The three curves are identical, which means that the SF_6 was well-mixed in the office. Next, the curve in the decay period in Location 2 was used for regression in Figure 9(b) to fit the decay equation [26]:

$$\mathrm{C(t)} = C_R e^{-\lambda_R t} \tag{21}$$

where $C_R(ppm)$ was the initial SF_6 concentration in the decay period, and $\lambda_R(s^{-1})$ was the air change rate. We obtained

$$\mathrm{C(t)} = 5.26(ppm)e^{-8.65\times10^{-5}(s)t} \tag{22}$$

The corresponding air infiltration was 0.311 h^{-1} or $Q_{f,measured}$ = 25.7 m^3/h. Compared with the infiltration rate calculated by the proposed method, the relative error was only 3.0%. This effort further validated the proposed method for a realistic scenario.

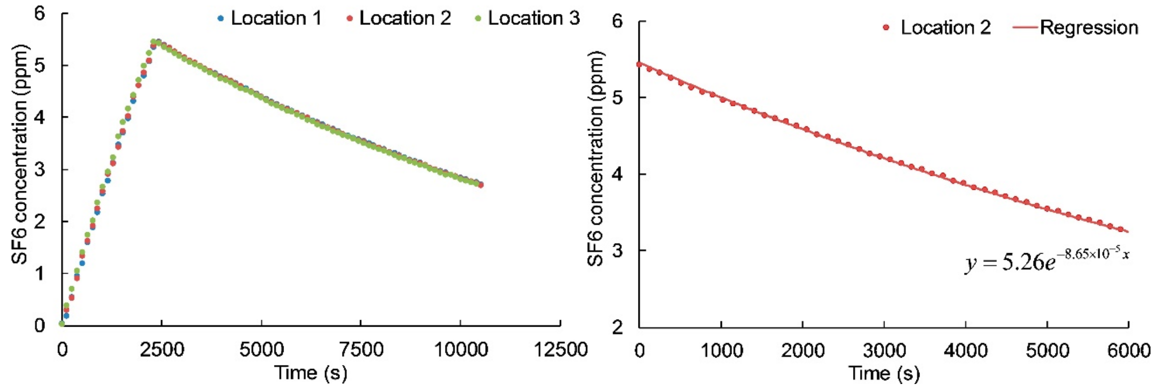

(a) (b)

Figure 9. Measured SF_6 concentration: (a) at three locations and (b) the regression results for the concentration at Location 2.

4. Discussions

The developed method made several assumptions. For example, this study assumed the flow through the crack to be laminar because the crack would be rather small ($D >> L_c$). Using the experiment setup in the chamber as an example, we have L_c = 1 *mm* and U_m = 2.5 *m/s* when the leaked airflow rate was 75 *L/min*. Then the Reynolds number is Re = 1655 that confirms the assumption of laminar flow. In reality, the crack could be even smaller that leads to smaller Reynolds number. However, some of the assumptions may bring unknown errors or limit the applicability of the developed method. For example, if the path way is not straight, it should not be a major problem as soon as $D >> L_c$ so the method would not generate a notable error. However, if the crack size is not uniform and the size in reality is difficult to find, the corresponding potential errors from this assumption could be a subject for further investigation.

This study assumed the flow over the wall surface to be parallel flow over an isothermal flat plate. A wall in reality can hardly be isothermal, which bring in unknown errors. However, such unknown errors would be minimal if the flow near a wall is in the turbulent boundary layer, where the heat convection coefficient varies little.

This study neglected the solar radiation that was acceptable if the method was applied at night. During night, the sky radiation may not have a major impact on the accuracy in most conditions. If one need to measure the leakage of the roof, the sky radiation should be included in Eq. 13. This study assumed that all heat transfer through the wall is done by the leaked air flow. This assumption is acceptable only if the indoor and outdoor thermal environments do not change much or there is little heat storage. Therefore, this study recommends using the developed method if the thermal environment is close to steady state and for light construction.

For the experiment in the environmental chamber, this study established a scaled model (the box) to investigate air infiltration. To determine whether the box was comparable to an actual building, we used the measured data to identify the coefficients in the power law equation [27] for calculating the air infiltration rate:

$$Q_f = C_f \Delta P^n \tag{23}$$

where C_f ($m^3 s^{-1} Pa^{-n}$) is the flow coefficient and n is the flow exponent. According to the linear regression shown in Figure 10, the flow exponent was $n = 0.7968$ and the flow coefficient was 0.000424 $m^3 s^{-1} Pa^{-n}$. The flow exponent was within the range (0.5–0.9) found in literature [28].

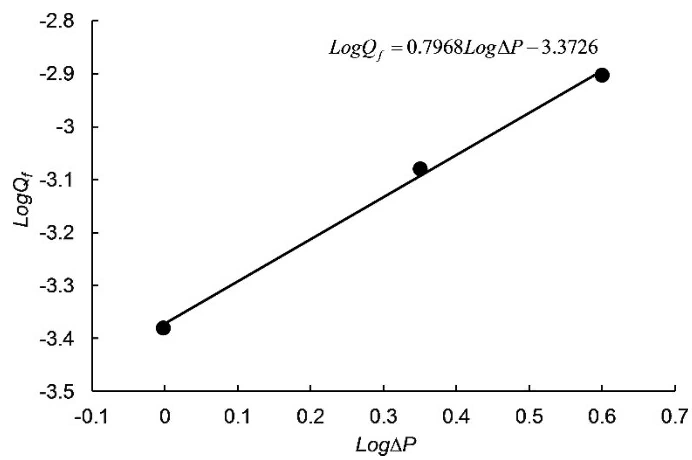

Figure 10. Relationship between air infiltration rate and indoor-outdoor pressure difference in the environmental chamber.

Next, this study calculated the normalized leakage (NL) [28], which is defined as:

$$\mathrm{NL} = 1000 \frac{ELA}{A_f} \left(\frac{H}{0.25m}\right)^{0.3} \tag{24}$$

where A_f is the floor area, H the building height, and ELA [28] the effective leakage area defined as:

$$\mathrm{ELA} = C_f \Delta P_R^{n-1/2} \left(\frac{\rho}{2}\right)^{1/2} \tag{25}$$

With $\Delta P_R = 4$ Pa, the calculated NL was 1.24 for the box, while the NL for most buildings in the U.S. is between 0 and 3 [28]. Therefore, the experimental setup in this study was comparable with realistic conditions.

The proposed method failed to accurately predict the crack size when the air infiltration rate was 75 L/min for the box in the environmental chamber. To identify the reasons for the failure, we conducted CFD simulations of the airflow and heat transfer within the duct, box, and test chamber for Scenario 3. The conjugate heat transfer within the box wall was also simulated. The computational domain included only the environmental chamber. Table 3 summarizes the thermal boundary conditions used, where the wall temperatures were measured by an infrared thermometer.

Table 3. Thermal boundary conditions for the environmental chamber.

Boundary	T (*K*)	Boundary	T (*K*)
North wall	297.2	Windows	299.2
South wall	297.2	Floor	296.5
West wall	296.8	Ceiling	297.7
East wall	296.6	Duct	adiabatic
North inlet air	294.6	South inlet air	293.0

This study conducted a transient CFD simulation with the re-normalization group (RNG) k-ε model [29] using ANSYS Fluent [30]. The model is widely used for simulating the turbulence in indoor airflow [31]. The Boussinesq approximation [32] was adopted to simulate the buoyancy effect. The wall Prandtl was set at $Pr_t = 0.01$ to ensure that the wall function would generate the correct heat transfer according to Zhang et al. [33]. We used a semi-implicit method for pressure-linked equations (SIMPLE) algorithm [34] to couple the velocity and pressure. The PRESTO! scheme was used to discretize the pressure term, and a second-order upwind scheme to discretize the other parameters. The solution was considered to be converged when the sum of the normalized residuals for all the cells became less than 10^{-6} for energy and 10^{-4} for all other variables.

Figure 11 shows a structured grid with 2.5 million cells for the computational domain according to our grid independence test. The grid around the crack and boundaries was refined. This study ran a steady CFD simulation first to initialize the flow variables, such as air pressure, velocity, and temperature. Next, we conducted transient simulation for two time constants ($\tau = 100\ s$) to obtain statistically steady data, and for another time constant to obtain a time-averaged solution. The time step size was 0.1 s. To validate the CFD simulation, we compared the predicted air velocity profiles at four typical locations (Locations 1, 4, 7, and 10) with the experimental data, as shown in Figure 12. The CFD simulation agreed well with the experimental data. This study did not compare the computed and measured air temperature because the air temperature variation along the vertical direction was less than 0.5 K. However, Figure 13 shows the computed temperature distributions on the wall with the crack. According to the simulation results, $T_{w,in} = 25.7\ ^oC$ and $T_{w,out} = 23.9\ ^oC$, which are almost the same as the measured data: $T_{w,in} = 26.0\ ^oC$ and $T_{w,out} = 24.0\ ^oC$.

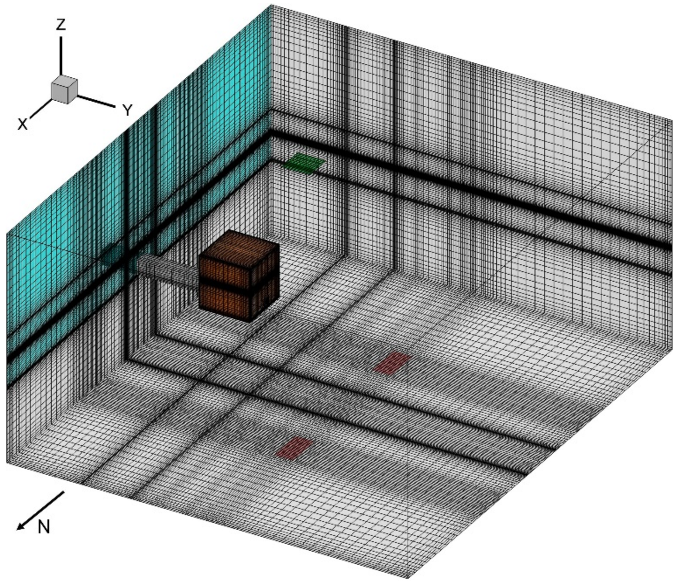

Figure 11. Structured grid for the environmental chamber.

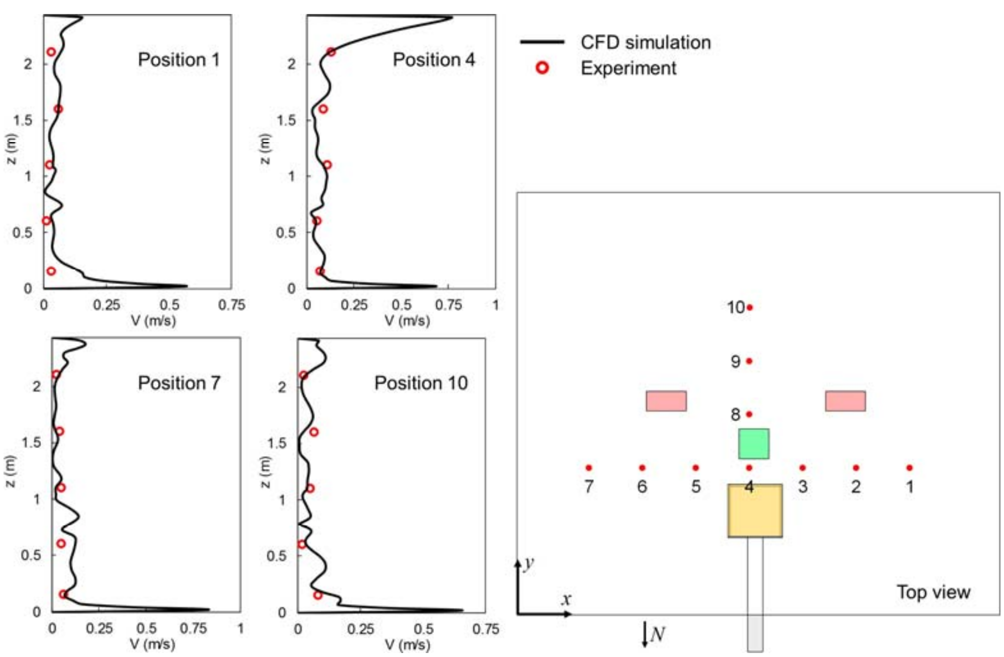

Figure 12. Comparison of the computed air velocity profiles from floor to ceiling with the experimental data in different locations (The coordinates of location 4 were (2.463, 1.492) and the distance between neighboring locations was 0.5 m).

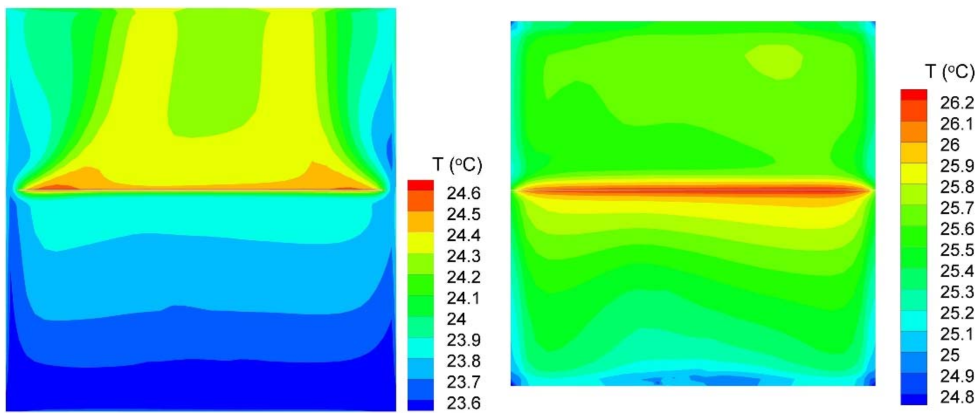

Figure 13. Computed temperature distributions on the wall with the crack: (left) outside surface and (right) inside surface.

The CFD simulation provided the heat exchange between the ambient air and the box wall surface. According to the CFD results, $Q_{in,exp}$ + $Q_{out,exp}$ = 0.343 W in Eq. 13, while the measured data were $Q_{in,exp}$ + $Q_{out,exp}$ = 0.368 W, which shows that the CFD and measured results were similar for heat flux. However, $T_{l,in} - T_{l,out}$ was 1.0 K according to the CFD simulation, whereas the measured temperature difference was 1.8 K. When we used $T_{l,in} - T_{l,out}$ = 1.0 K in Eq. 13, the corresponding calculated crack size was $L_{c,calculated}$ = 0.9 mm, which was very close to the actual crack size. Therefore, the errors in the calculations for Scenarios 3 and 6 in Section 3.1 may have been due to inaccurate estimation of the leaked air temperature. But note that 75 L/min corresponds to 3.6 h^{-1} that is unlikely to happen in reality, this study believes that there is no difficulty in estimating the leaked air temperature when the developed method is applied in a real condition. That is the reason for using the air infiltration in an office for demonstration.

For the experiment in an office, the indoor/outdoor temperature difference was about 9 K and the developed method was still able to accurately identify the air infiltration rate, which means the method is applicable for conditions with low indoor/outdoor temperature difference. However, a larger indoor/outdoor temperature difference would weaken the errors and uncertainties in the developed method and further lead to better accuracy in measuring the air infiltration. If there are multiple surfaces with cracks, one can apply the method to the whole surface to obtain the total air infiltration rate or part of the surface to obtain the regional air infiltration rate. The test in this office also showed that the developed method required only one person and half a day to get the job done. Besides, the equipment used in developed method was light weight and easy for installation comparing with the traditional blower door method.

With all the above-mentioned uncertainties and limitations, further validations in different buildings are necessary to improve the developed method. These validations could be used to modify the developed method by using machine learning or data mining technique.

5. Conclusions

This study developed a novel method for measuring the air infiltration rate in buildings. The proposed method is able to determine the effective crack size and air infiltration rate by using the air temperature distributions on the interior and exterior surfaces of a wall containing a crack, indoor and outdoor air temperatures, indoor-outdoor pressure difference, and indoor and outdoor air velocities.

The proposed method was validated by the measured crack size in a small box installed in an environmental chamber and by the measured infiltration rate in an office with the use of the tracer-gas decay method. The proposed method was able to predict the crack size with a relative error of less than 20% when the air infiltration rate was low. For a higher infiltration rate, the error was larger, possibly because of inaccurate estimation of the leaked air temperature. This inaccuracy was identified by detailed CFD simulation of airflow and temperature distribution in the environmental chamber containing the box. The proposed method estimated the air infiltration rate in the office with a relative error of only 3%.

This study confirmed that the small box in the environmental chamber could be used to simulate infiltration in an actual room. This is because the coefficients obtained in the power law equation for calculating the air infiltration rate were in the same range as those in full-scale buildings found in the literature. Furthermore, the normalized leakage determined by using the box data was also within the normal range found in the literature.

Acknowledgement

This research is partially supported by the national key R&D project on Green Buildings and Building Industrialization of the Ministry of Science and Technology, China, through Grant No. 2016YFC0700500; the National Natural Science Foundation of China through Grant No. 51678395; and the key project of the Applied Basic and Frontier Technology Research Program of Tianjin Commission of Science and Technology, China, through Grant No. 15JCZDJC40900.

Nomenclature

Symbol definition

A	wall area
C	species concentration
C_f	flow coefficient
C_p	specific heat in constant pressure
D	wall thickness
ELA	effective leakage area
h	heat convective coefficient
H	room height

L_c	crack height
n	flow exponent
Nu	Nusselt number
NL	normalized leakage
P	air pressure
Pr	Prandtl number
Q	heat flux
Q_f	leaked airflow rate
Re	Reynolds number
t	time
T	air temperature
u, v, w	velocity component in x, y, and z direction, respectively
V	air velocity
x, y, z	index of coordinates
ρ	air density
μ	dynamic viscosity
λ	air change rate
τ	time constant

Subscripts

c	critical value
in	value at indoor side
out	value at outdoor side
l	value for leaked air
m	mean value
R	reference value
w	value at the wall
∞	value for ambient air

References

[1] US EIA. 2015. “Annual Energy Outlook.” US Energy Information Administration: Washington.

[2] DOE. 2015. “Building Energy Data.”

[3] Sandberg, P. I., and E. Sikander. 2005. “Airtightness issues in the building process.” *Proceedings of the 7th Symposium on Building Physics in the Nordic Countries* 420–427.

[4] Emmerich, S. J., and A. K. Persily. 1998. “Energy impacts of infiltration and ventilation in US office buildings using multizone airflow simulation.” *Proc.IAQ Energy* 98: 191–206.

[5] Brinks, P. 2013. “Astron Energy Report and Database Internal Report,” not published. *Luxembourg, Diekirch, Lindab SA*.

[6] Brinks, Pascal, Oliver Kornadt, and René Oly. 2015. “Air infiltration assessment for industrial buildings.” *Energy and Buildings* 86: 663–676.
[7] Kirkwood, RC. 1977. “Fuel consumption in industrial buildings.” *Building Services Engineer* 45 (3): 23–31.
[8] Nevrala, DJ, and DW Etheridge. 1977. “Natural ventilation in well-insulated houses.” In *Proceedings of International Centre for Heat and Mass Transfer, International Seminar, UNESCO, Dubrovnik, Croatia,* Vol. 29.
[9] Caffey, GE. 1979. “Residential air infiltration.” *ASHRAE Trans* 85 (part 1).
[10] NIST (National Institute of Standards and Technology). 1996. “NIST estimates nationwide energy impact of air leakage in U.S. buildings.” *Journal of Research of the NIST* 101 (3): 423.
[11] Jokisalo, Juha, Targo Kalamees, Jarek Kurnitski, Lari Eskola, Kai Jokiranta, and Juha Vinha. 2008. “A comparison of measured and simulated air pressure conditions of a detached house in a cold climate.” *Journal of Building Physics* 32 (1): 67–89.
[12] Airaksinen, M, P Pasanen, J Kurnitski, and O Seppänen. 2004. “Microbial contamination of indoor air due to leakages from crawl space: A field study.” *Indoor Air* 14 (1): 55–64.
[13] Rantala, Jukka, and Virpi Leivo. 2009. “Heat, air, and moisture control in slab-on-ground structures.” *Journal of Building Physics* 32 (4): 335–353.
[14] Chen, Chun, and Bin Zhao. 2011. “Review of relationship between indoor and outdoor particles: I/O ratio, infiltration factor and penetration factor.” *Atmospheric Environment* 45 (2): 275–288.
[15] Lstiburek, Joseph, Kim Pressnail, and John Timusk. 2002. “Air pressure and building envelopes.” *Journal of Thermal Envelope and Building Science* 26 (1): 53–91.
[16] Hagentoft, C-E, and E Harderup. 1996. “Moisture conditions in a north facing wall with cellulose loose fill insulation: Constructions with and without vapor retarder and air leakage.” *Journal of Thermal Insulation and Building Envelopes* 19 (3): 228–243.
[17] Younes, Chadi, Caesar Abi Shdid, and Girma Bitsuamlak. 2012. “Air infiltration through building envelopes: A review.” *Journal of Building Physics* 35 (3): 267–302.
[18] Blomsterberg, A. 1977. “Air Leakage in Dwellings.” *Dept. Bldg. Constr. Report* (15).
[19] Harrje, DT, A Blomsterberg, and A Persily. 1979. “Reduction of Air Infiltration Due to Window and Door Retrofits.” *CU/CEES Report* 85.
[20] Sherman, Max. 1995. “The use of blower-door data.” *Indoor Air* 5 (3): 215–224.
[21] ASTM, E. 2011. “Standard test methods for determining airtightness of buildings using an orifice blower door.” *ASTM International*, West Conshohocken, PA.
[22] Kalamees, Targo. 2007. “Air tightness and air leakages of new lightweight single-family detached houses in Estonia.” *Building and environment* 42 (6): 2369–2377.
[23] Dufour, Marianne Bérubé, Dominique Derome, and Radu Zmeureanu. 2009. “Analysis of thermograms for the estimation of dimensions of cracks in building envelope.” *Infrared Physics & Technology* 52 (2): 70–78.
[24] Qi, Te. 2012. “Inverse modeling to predict effective leakage area.” Ph.D. thesis. Georgia Institute of Technology.

[25] Bergman, Theodore L, and Frank P Incropera. 2011. *Fundamentals of heat and mass transfer*. John Wiley & Sons.
[26] Sherman, Max H. 1990. "Tracer-gas techniques for measuring ventilation in a single zone." *Building and Environment* 25 (4): 365–374.
[27] Walker, Iain S, David J Wilson, and Max H Sherman. 1998. "A comparison of the power law to quadratic formulations for air infiltration calculations." *Energy and Buildings* 27 (3): 293–299.
[28] Sherman, Max, and Darryl Dickerhoff. 1994. "Air-tightness of US dwellings." In *Document-air Infiltration Centre AIC PROC,* 225–225. OSCAR FABER PLC.
[29] Yakhot, Victor, and Steven A Orszag. 1986. "Renormalization-group analysis of turbulence." *Physical Review Letters* 57 (14): 1722.
[30] Fluent, Ansys. 2009. "12.0 Theory Guide." *Ansys Inc* 5.
[31] Zhang, Zhao, Wei Zhang, Zhiqiang John Zhai, and Qingyan Yan Chen. 2007. "Evaluation of various turbulence models in predicting airflow and turbulence in enclosed environments by CFD: Part 2 Comparison with experimental data from literature." *HVAC&R Research* 13 (6): 871–886.
[32] Boussinesq, Joseph. 1903. *Théorie analytique de la chaleur: mise en harmonie avec la thermodynamique et avec la théorie mécanique de la lumière*. Vol. 2. Gauthier-Villars.
[33] Zhang, Tengfei Tim, Hongbiao Zhou, and Shugang Wang. 2013. "An adjustment to the standard temperature wall function for CFD modeling of indoor convective heat transfer." *Building and Environment* 68: 159–169.
[34] Patankar, Suhas V, and D Brian Spalding. 1972. "A calculation procedure for heat, mass and momentum transfer in three-dimensional parabolic flows." *International Journal of Heat and Mass Transfer* 15 (10): 1787–1806.